TIME-DEPENDENT MICRO MECHANICS IN DAMAGED HIGH-TEMPERATURE CERAMIC COMPOSITES

A. EL-AZAB and N. M. GHONIEM
Mechanical and Aerospace Engineering Department
University of California, Los Angeles
California 90095-1795

ABSTRACT

Under monotonic loading of unidirectional ceramic-matrix composites, it has been observed that periodic matrix cracking takes place if the matrix strain-to-failure is below that of the fibers. Furthermore, it has been found that interface debonding, frictional slip and the subsequent bridging of matrix cracks control the overall response of this class of materials. At elevated temperatures, however, fiber and/or matrix creep is expected to dominate the micro mechanical behavior and, in turn, the macroscopic deformation response of the composite. In this paper, a micro mechanical model is developed to study the effects of fiber creep on fiber-matrix interface debonding and fiber frictional slip. The model is particular to composite systems whose fibers exhibit much faster creep rates in comparison with matrices. The model is applied to predict the creep response of composites loaded beyond the matrix cracking stress. It is found that the macroscopic creep response is characterized by a secondary creep regime which is associated with slow propagation of interface debonding cracks, followed by a tertiary creep regime during which rapid growth of debonding represents an instability mechanism.

INTRODUCTION

Ceramic-matrix fiber-reinforced composites exhibit single and multiple fracture behavior under monotonic loading (Aveston et al., 1971). In the present work, focus will be on ceramic composite systems which exhibit multiple matrix fracture, i.e., fibers can sustain the load carrying capability of the composite following the first matrix cracking event. Such composite systems are characterized by fibers which have larger strain-to-failure in comparison with the matrix. Nicalon-CVD (CVI) SiC composites exhibit this type of behavior. In this class of composites, interface debonding and frictional slip between fibers and matrix are critical micro mechanical phenomena which control matrix cracking and hence the low-temperature strength and toughness of these composites. The work of Aveston et al. (1971), Aveston and Kelly (1973), Kelly (1976), Budainsky et al. (1986) has focused on predictions of the matrix cracking stress under different interfacial conditions. Several micro mechanical models for fiber debonding and slip have been developed by Marshall et al.(1985), Gao et al. (1988), Sigl and Evans (1989), Hutchinson and Jensen, (1990), Kim et al. (1991) and Zhou et al. (1991). These models are generally time-independent and were developed to obtain load-displacement relationship at the single fiber level, and to predict interfacial properties in fiber composites.

Ceramic-matrix fiber-reinforced composites such as SiC-SiC are under development for high-temperature structural applications (e.g., jet engines (Evans, 1994) and fusion reactor structures (Najmabadi et al. 1995)). Elevated-temperature mechanical properties of these materials are expected to be influenced by the time-dependent inelastic response of the micro constituents of the composite (fibers, matrix and interfaces). For Nicalon (SiC fiber)-CVD (CVI) SiC composites, it has been experimentally observed that the fibers exhibit a temperature-threshold for creep which is lower than that of CVD SiC. This experimental finding has triggered experimental (Henager and Jones, 1993) and theoretical (El-Azab, 1994) high-temperature time-

dependent matrix crack growth studies is Nicalon-SiC composites. A time-dependent micro mechanics model was developed by El-Azab (1994) to obtain the relationship between the crack bridging tractions and the crack opening displacement, which considers fiber creep in the crack bridging zone to result in a time-dependent response of loaded matrix cracks. The present work adopts a similar procedure to study the overall load-deformation response of one dimensional ceramic composites with periodic matrix cracks and creeping fibers. Figure 1 illustrates the problem studied here. The composite is assumed to be loaded beyond matrix cracking stress and fibers are carrying the full load wherever the matrix is cracked. The goal of the micro mechanical analysis conducted here is to predict the overall load-displacement response, and hence the macroscopic creep strain as a function of time and temperature for Nicalon-SiC composites. Following this introduction, a short description of fiber and matrix creep characteristics is presented. The underlying assumptions for the present model and its development are then included and the paper concludes with a thorough presentation and discussion of the model results and conclusions.

CREEP CHARACTERISTICS OF CVD SiC AND NICALON FIBERS

CVD SiC has been tested for creep in compression in the temperature range 1550-1750°C (Carter and Davis, 1984) and in bending in the range 1200-1500°C (Gulden and Driscoll, 1971). The bending creep data are considered here. The creep rate of CVD SiC in compression exhibits a power law dislocation mechanism-type creep with a stress exponent of 2.5, while the data of Gulden and Driscoll (1971) exhibited a diffusional creep law of the form

$$\dot{\varepsilon}_c = 13.3 \frac{\sigma D_a \Omega_a}{kTd_g^2} \tag{1}$$

where σ is the applied stress, D_a is the diffusion coefficient for the rate-controlling species, Ω_a is the atomic volume, k is the Boltzmann constant, T is the absolute temperature and d_g is the grain size. An activation energy of 640 ± 88 KJ/mole was measured. Nicalon fibers were also tested for creep by DiCarlo and Morscher (1991) (see also DiCralo (1994)). It is found that the creep strain, ε_c, for Nicalon fibers is given as function of stress, time and temperature by

$$\varepsilon_c = A\sigma \exp\left(\frac{-Q}{R_g T}\right) t^p \tag{2}$$

where R_g is the gas constant. For stress in MPa, temperature in K and time in seconds, A = 8.316, and the apparent activation energy is Q = 2.91 KJ/mole and p = 0.4. The stress exponent for Nicalon fibers is slightly different from unity (DiCralo, 1994), but considered to be unity in the present analysis to allow the use of linear viscoelasticity theory. Creep data for Nicalon fibers and CVD SiC were compared (El-Azab and Ghoniem, 1995) and it is found that Nicalon fibers exhibited creep rates which are several orders of magnitude higher than CVD SiC creep rates for the same temperature and applied stress. It is thus concluded that, as far as Nicalon-CVD SiC composite is concerned, the matrix creep can be totally ignored in comparison with fiber creep below 1400 °C.

PROBLEM DESCRIPTION

Figure 1 shows a schematic of a unidirectional fiber composite, which is loaded beyond the matrix cracking stress. The matrix is periodically cracked and fibers are bridging matrix crack faces. The matrix crack density is a function of the applied stress, σ_a, and the mean distance between two matrix cracks is denoted by $2L$. Composites with initially bonded interfaces are considered. In such ceramic composites, residual misfit stresses exist, which arise during

manufacturing. In the present analysis, an inelastic strain component, denoted by ε_{th} , is assumed to represent the residual misfit and considered to be a part of the matrix strain. Thus, an initial macroscopic strain component in the composite will be present, and must be accounted for in calculating the composite macroscopic strains under externally imposed loads. This will be clarified later during the analysis. Now assume that the composite temperature is above the temperature threshold for fiber creep, and the applied stress, σ_a, is acting along the fiber direction. Due to symmetry, consider only a composite length L, (i.e., half the distance between two matrix crack) starting at one of the matrix cracks. The composite is expected to respond in the following way (see Figures 1 and 2). Between the matrix crack faces, the applied stress is fully taken by fibers, so that the local fiber stress, σ_f, is given by

$$\sigma_f = \sigma_a / f \tag{3}$$

where f is the fiber area fraction on the matrix crack. In unidirectional composites, f itself is the volume fraction of fibers. At the onset of matrix cracking (initial loading), the fiber-matrix interface is debonded over a certain length ℓ. Over this length, fibers undergo slip relative to the matrix so that at matrix crack surfaces fibers are partially pulled-out of the matrix. This partial slip process contributes to the overall macroscopic strain of the composite and depends on interfacial conditions, the residual misfit strain, and the applied load. Over the distance $L - \ell$ slip between fibers and matrix is not allowed and the axial deformation of the composite over this length is more restricted. Fiber creep will primarily lead to relaxation of the residual misfit strains and an additional deformation in response to the applied load. Therefore, fiber creep will result in a time-dependent overall deformation under constant applied stress. Calculating this deformation for the composite, however, is not straightforward and requires detailed micro mechanical analysis of the associated time-dependent debonding and slip processes in the composite, which is the main objective of the present work.

MODEL ASSUMPTIONS AND DEVELOPMENT

Model Formulation

The composite (fiber/matrix) cylinder depicted in Figure 2 is used to simulate the response of the macroscopic composite. Due to symmetry conditions, a length L is considered for analysis. The fiber radius is denoted by R and the outer radius of the matrix around the fiber is $\bar{R}_o$. This geometrical idealization has been used by many authors to model the micro mechanics of fiber debonding and slip (Marshall et al., 1985; Gao et al., 1988; Sigl and Evans 1989; Hutchinson and Jensen, 1990; Kim at al., 1991 and Zhou et al., 1991), and recently by El-Azab (1994). The work mentioned above has only dealt with the micro mechanics problem under static conditions with no fiber creep. The present work is a generalization of the previous literature to include the effects of fiber creep on the micro mechanical response.

Hutchinson (1994) used the concentric cylinder model as geometrical idealization for composites with hexagonal arrays of fibers in matrices, with periodic boundary conditions on the cylinder side of the form

$$u_r = const, \text{ and } \quad \sigma_{rz} = 0 \quad \text{at} \quad r = \bar{R}_o \tag{4}$$

where u_r is the radial displacement, and the constant is the radial displacement above the debond front. The stress components have their conventional meaning for cylindrical coordinates (see Figure 2). At the matrix crack surface, the fiber end is subject to a stress σ_f, and the matrix is stress free. At $z = L$ the composite cylinder is subject to a zero axial displacement condition $u_z = 0$. If $\sigma_r(\bar{R}_o)$ is take to be zero, the model represents an isolated cylindrical cell and is more suitable for the single fiber composite analysis. For simplicity, the isolated cylindrical

cell boundary conditions are considered here. An interface debonding zone develops whose length is time-dependent, and over which relative slip is permissible between fibers and matrix. The interfacial friction is assumed to follow a Coulomb-type law of the form

$$\tau = -\mu q \tag{5}$$

where q is the normal pressure at the interface, and μ is a friction coefficient. In this model, we neglect gradients in shear stresses in the matrix compared with normal stresses over the debonded zone, which is valid as long as the axial stress in the matrix varies slowly over distance comparable to the fiber radius. In this case, the axial, radial and azimuthal stress at any section normal to the z-axis are characterized by a Lamé problem solution. The fiber and matrix stresses are given by

$$\sigma_r^f = \sigma_\theta^f = q$$

$$\sigma_r^m = \frac{q}{1-f}\left[\left(\frac{R}{r}\right)^2 - f\right] \quad \text{and} \quad \sigma_\theta^m = \frac{-q}{1-f}\left[\left(\frac{R}{r}\right)^2 + f\right] \tag{6}$$

where superscripts (subscripts) f and m refer to fiber and matrix, respectively, and r is the radial distance from the fiber center. It is to be mentioned that all stresses, strains and displacements depend on time, t, and the axial coordinate, z. The corresponding matrix strains are given by

$$\varepsilon_{ij}^m = \varepsilon_{th}\delta_{ij} + \frac{1+\nu_m}{E_m}\sigma_{ij}^m - \frac{\nu_m}{E_m}\sigma_{kk}^m\delta_{ij} \tag{7}$$

where the non-elastic term ε_{th} is associated with normal components only, which represents an isotropic shrinkage term. This induces matrix clamping around the fiber. With the current formulation of the problem, only normal stresses in fiber and matrix are considered (Lamé problem). The detailed form for fiber strains are written as

$$\varepsilon_\theta^f = \varepsilon_r^f = \frac{1}{E_f}\left[(1-\nu_f)q - \nu_f\sigma_z^f\right] + \int_0^t \dot{J}(t-t')\left[(1-\nu_{fc})q(t') - \nu_{fc}\sigma_z^f(t')\right]dt'$$

$$\varepsilon_z^f = \frac{1}{E_f}\left[\sigma_z^f - 2\nu_f q\right] + \int_0^t \dot{J}(t-t')\left[\sigma_z^f(t') - 2\nu_{fc}q(t')\right]dt' \tag{8}$$

where ν_{fc} is the Poisson's ratio of fibers for creep strains, $J(t)$ is the creep compliance, which is defined by the creep strain at time t per unit stress in a one dimensional creep experiment, which is given by Eq. (2). The first term to the right hand side of any of Eqs. (8) represents the elastic strain component, while the second term represents the creep strain component.

The solution for the stress and strain distributions are found in two different regions: $0 < z < \ell$ and $\ell < z < L$. For $0 < z < \ell$, the field quantities are functions of time and the axial coordinate z, and the condition of continuity of radial displacement at the fiber-matrix interface must be satisfied. This condition is written as

$$\varepsilon_\theta^f(z, R, t) = \varepsilon_\theta^m(z, R, t) \tag{9}$$

The axial equilibrium for both fiber and matrix is also written as

$$\frac{\partial\sigma_z^f}{\partial z} = \frac{-2\tau}{R} = -\frac{1-f}{f}\frac{\partial\sigma_z^m}{\partial z} \tag{10}$$

For $\ell < z < L$, the field quantities are independent of the axial coordinate and both the radial and axial displacements are continuous at the interface. The axial equilibrium condition is given by

$$f\sigma_z^f + (1 - f)\sigma_z^m = \sigma_a \tag{11}$$

For $0 < z < \ell$, by using Eq. (5), the condition (9), and the equilibrium Eq. (10), the following equation can be obtained for the interface pressure $q(z, t)$

$$\frac{\partial q(z, t)}{\partial z} = \frac{2\mu c_1}{R} q(z, t) + c_o \int_{t_d}^{t} \dot{J}(t - t') \times \left[\left(1 - \nu_{fc}\right) \frac{\partial q(z, t')}{\partial z} - \frac{2\mu \nu_{fc}}{R} q(z, t') \right] dt' \tag{12}$$

where c_o and c_1 are given in the appendix. The lower limit of the integral t_d represents the time at which the debonding crack front reaches a particular location z and depends on z itself, since the debond crack is assumed propagating. Eq. (12) can be solved by the method of Laplace transform, where the Laplace transform of the convolution integral can be found by shifting its limits by an amount t_d. Details of the inversion are given by El-Azab (1994), and the transformed equation is written as

$$\frac{d\hat{q}(z, s)}{dz} = \frac{2\mu}{R} \left[\frac{c_1 - c_o \nu_{fc} s\hat{J}(s)}{1 - c_o(1 - \nu_{fc}) s\hat{J}(s)} \right] \hat{q}(z, s) = \frac{2\mu\hat{\alpha}(s)}{R} \hat{q}(z, s) \tag{13}$$

where s is the Laplace parameter. Eq. (13) has a solution of the form

$$\hat{q}(z, s) = \hat{q}(0, s) \exp\left(\frac{2\mu\hat{\alpha}(s) z}{R} \right) \tag{14}$$

By applying the continuity of the radial displacement at $z = 0$, and taking the Laplace transform of the resulting relationship, it can be shown that $\hat{q}(0, s)$ is given by

$$\hat{q}(0, s) = \frac{c_3}{c_4 + c_3(1 - \nu_{fc}) s\hat{J}(s)} \frac{\varepsilon_{th}}{s} + \frac{c_2 + c_3 \nu_{fc} s\hat{J}(s)}{c_4 + c_3(1 - \nu_{fc}) s\hat{J}(s)} \frac{\sigma_f}{s} \tag{15}$$

where c_2, c_3 and c_4 are included in the appendix. For further manipulation, let Eq. (15) be rewritten in the form

$$\hat{q}(0, s) = \hat{\alpha}_1(s) \frac{\varepsilon_{th}}{s} + \hat{\alpha}_2(s) \frac{\sigma_f}{s} \tag{16}$$

This equation can not be analytically inverted to the time domain. An approximate analytical inversion method (Schapery, 1962 and Pipkin, 1986) is used to obtain the time-dependent solution. Leaving out details, the final form of the time-dependent axial distribution of the interface pressure over the debonded zone is given by

$$q(z, t) = \left[\alpha_1(t) \varepsilon_{th} + \alpha_2(t) \sigma_f \right] \exp\left(\frac{2\mu\alpha(t) z}{R} \right) \tag{17}$$

where $\alpha(t)$, $\alpha_1(t)$ and $\alpha_2(t)$ are obtained from their Laplace transform by replacing $s\hat{J}(s)$ by $J(t)$ according to the Schapery's inversion formula (Schapery, 1962) $J(t) \approx \left[s\hat{J}(s) \right]_{s=0.5/t}$, which is a good approximation if $J(t)$ behaves as t^p with $p \sim 0.4$. Using the axial equilibrium conditions, it can be shown that the axial fiber and matrix stress distributions can be written as

$$\sigma_z^f = \sigma_f + \frac{\alpha_1(t) \varepsilon_{th} + \alpha_2(t) \sigma_f}{\alpha(t)} \left[\exp\left(\frac{2\mu\alpha(t) z}{R} \right) - 1 \right],$$

$$\text{and} \qquad \sigma_z^m = \frac{f}{1 - f} \left(\sigma_f - \sigma_z^f \right) \tag{18}$$

It will be shown later that the three components of fiber stress (σ_z^f and $q(z,t) = \sigma_\theta^f - \sigma_r^f$,) are sufficient to predict the overall macroscopic strain of the composite.

The solution in the interval $\ell < z < L$ can be obtained by using the axial equilibrium condition (11), and the continuity of the radial and axial displacements at the fiber-matrix interface. The final results for the interface pressure and the axial fiber stress are found to have the form

$$\sigma_z^f(t) = A_1(t)\sigma_a + B_1(t)\varepsilon_{th}, \text{ and } q(t) = A_2(t)\sigma_a + B_2(t)\varepsilon_{th} \quad (19)$$

where $A_1(t)$, $B_1(t)$, $A_2(t)$ and $B_2(t)$ are given in the appendix.

Debonding Propagation

At the onset of matrix cracking (upon applying the external load), the fiber-matrix interface is debonded over an initial length $\ell(0)$, if the applied fiber stress is above the debonding threshold. Due to fiber creep, the interface debonding crack propagates due to relaxation of the interfacial pressure. The time-dependent debond crack length is found in the present study by studying the energetics of the composite cylinder loaded under fiber creep condition. It is possible to determine the debond length in this case, since the interfacial friction energy dissipation term depends on the debond crack length as a characteristic length. Details of the derivations are found elsewhere (El-Azab, 1994), and the time-dependent debonding criterion is found to have the form

$$4\Im_d = R\sigma_f \frac{d\delta^e}{d\ell} + 2\mu \frac{du_s^e}{d\ell} \int_0^t q(z,t)dz \quad (20)$$

in which $\Im_d$ is the interface debonding energy, δ^e is the elastic fiber displacement component at $z = 0$, which is given by the integral of the elastic axial strain component of the fiber, u_s^e is the relative slip between fiber and matrix (not including the slip component associated with fiber creep). δ^e and u_s^e are defined by

$$\delta^e = \int_0^t \varepsilon_z^{f,e}(z,t)dz + \int_\ell^L \varepsilon_z^{f,e}(z,t)dz, \text{ and}$$
$$u_s^e(z) = \int_z^t \left[\varepsilon_z^{f,e}(z',t) - \varepsilon_z^m(z',t)\right]dz \quad (21)$$

where the superscript e refers to non-creep components. The debond criterion (20) becomes identical to the debond criterion developed by Gao at al. (1988) if no creep effects are present. It can be shown that $\frac{d\delta^e}{d\ell}$ and $\frac{du_s^e}{d\ell}$ are dependent on the fiber and matrix stress components just below and just above the debonding front, which will be distinguished by the superscripts + and - , respectively. The final form of the debonding relationship is found to be

$$\frac{4\Im_d E_f}{R} = \sigma_f\left[\sigma_f^- - \sigma_f^+ - 2\nu_f(q^- - q^+)\right] - \left(\sigma_f - \sigma_f^-\right) \times \left[E_f\varepsilon_{th} + \sigma_f^- - 2\nu_f q^- - \frac{E_f}{E_m}\left(\sigma_m^- + \frac{2\nu_m f q^-}{1-f}\right)\right] \quad (22)$$

in which the subscripts f and m refer to fiber and matrix quantities, respectively, and, in addition to the interface pressure q^- and q^+, only axial fiber and matrix stress components are included. Eq. (22) is a transcendental relationship for the instantaneous debond length ℓ which

comes through the factor $\eta = \exp\left(\frac{2\mu\alpha(t)\ell}{R}\right)$ by substituting the solutions for q^-, σ_f^- and σ_m^- from Eqs. (17) and (18), respectively, at $z = \ell$.

In order to implement the relationship (20), the interface normal stress must be guaranteed to be compressive at all times below the debond front. Otherwise, a frictionless debonding relationship should be utilized. Under such circumstances, the debonding criterion will include the fiber radius R as the only characteristic length, which is found to have the form

$$\frac{4\,\mathfrak{I}_d E_f}{R} = \sigma_f\left[\sigma_f - \sigma_f^+ + 2\nu_f q^+\right] \tag{23}$$

This relationship gives no information about the debonding length.

Overall Composite Strain

So far the model development yields the axial distributions of the time-dependent stresses and the strain fields in the fiber and matrix. With the interface pressure being determined, other fiber stresses (radial and azimuthal) stresses can also be found. Referring to Figure 2, it can easily be shown that the apparent composite strain along the fiber direction is determined as the spatial average of the fiber strain over the representative interval $0 < z < L$, i.e.,

$$\bar{\varepsilon}(t) = \frac{1}{L}\int_0^t \varepsilon_z^f(z,t)\,dz + \frac{1}{L}\int_t^L \varepsilon_z^f(z,t)\,dz \tag{24}$$

which, based on Eq. (8), can be fully determined by utilizing the solution for $q(z,t)$ and $\sigma_z^f(z,t)$ over the intervals $0 < z < \ell$ and $\ell < z < L$. These solutions are given by Eqs. (17) and (18) and (19). By using these equations and carrying out the integrals, the overall composite axial strain can be determined from

$$\begin{aligned}
\bar{\varepsilon}(t) = \sigma_a\Bigg\{ & S_o(t)\frac{\ell(t)}{L} + S_1(t)\frac{R}{L}\frac{\left[\eta(\ell,t)-1\right]}{2\mu\alpha(t)} \\
& + \frac{R}{L}\frac{1}{2\mu}\int_0^t \dot{J}(t-t')S_2(t')\frac{\left[\eta(\ell,t')-1\right]}{\alpha(t')}\,dt' \\
& - \frac{\ell(t)}{fL}\int_0^t \dot{J}(t-t')\frac{\alpha_2(t')}{\alpha(t')}\,dt' \\
& + \left(1-\frac{\ell(t)}{L}\right)\left[P_1(t) + \int_0^t \dot{J}(t-t')P_2(t')\,dt'\right]\Bigg\} \\
+ \varepsilon_{th}\Bigg\{ & R_o(t)\frac{\ell(t)}{L} + R_1(t)\frac{R}{L}\frac{\left[\eta(\ell,t)-1\right]}{2\mu\alpha(t)} \\
& + \frac{R}{L}\frac{1}{2\mu}\int_0^t \dot{J}(t-t')R_2(t')\frac{\left[\eta(\ell,t')-1\right]}{\alpha(t')}\,dt' \\
& - \frac{\ell(t)}{L}\int_0^t \dot{J}(t-t')\frac{\alpha_1(t')}{\alpha(t')}\,dt' \\
& + \left(1-\frac{\ell(t)}{L}\right)\left[Q_1(t) + \int_0^t \dot{J}(t-t')Q_2(t')\,dt'\right]\Bigg\}
\end{aligned} \tag{25}$$

where $S_o(t)$, $S_1(t)$, $S_2(t)$, $P_1(t)$, $P_2(t)$, $R_o(t)$, $R_1(t)$, $R_2(t)$, $Q_1(t)$ and $Q_2(t)$ are included in the appendix. Prior to matrix cracking, the apparent axial composite strain can be determined from

$$\bar{\varepsilon}(t) = \sigma_a \left[P_1(t) + \int_0^t \dot{J}(t - t') P_2(t') dt' \right] + \varepsilon_{th} \left[Q_1(t) + \int_0^t \dot{J}(t - t') Q_2(t') dt' \right] \quad (26)$$

Expressions (25) and (26) yield the overall strain of the composite relative to the undeformed state. Assuming that no external stress is applied to the composite, and that fiber creep is not operable. In this case, the composite will undergo uniform axial deformation determined by the misfit effect, which can be either an overall shrinkage (if matrix is shrinking around fiber) or elongation (if fiber is expanding inside the matrix) in the axial direction. Let this strain component, which exists prior to application of the external load, be denoted by ε_o. If the composite temperature is raised so that fiber creep becomes operative and no external load is yet applied, misfit residual stresses will be relaxed, and the composite will undergo time-dependent deformation towards the unstrained condition of the matrix, which in the present case is elastic. This means that, under fiber creep conditions and in the absence of external loads, the composite undergoes time-dependent axial shrinkage, whose ultimate value is determined by the viscoelastic relaxation moduli (or creep compliances) of the fibers. If fibers behave as ideal viscoelastic fluid, ultimately the residual stresses can be completely relaxed. The second square bracket in Eq. (26) represents these effects. The value of this bracket at time zero determines ε_o, while its value at any time determines the time-dependent deformation of the composite along the axial direction as a function of time if fiber creep is operative under the influence of the residual misfit. In the present analysis, the overall creep deformation of the composite under the effect of external loads will be measured relative to the initial state of the composite prior to applying the external stress or triggering fiber creep, which are assumed to take place at the same moment. This means that the time-dependent overall creep strain of the composite along the axial direction, which is denoted by $\bar{\varepsilon}_c(t)$, is given by

$$\bar{\varepsilon}_c(t) = \bar{\varepsilon}(t) - \varepsilon_o \quad (27)$$

i.e., by the expression (25) (for cracked matrix) or (26) (for uncracked matrix) minus the value of the second square bracket in Eq. (26) at time zero. It can be easily verified that ε_o is given by

$$\varepsilon_o = \frac{B_1(0) - 2\nu_f B_2(0)}{E_f} \varepsilon_{th} \quad (28)$$

where $B_1(0)$ and $B_2(0)$ are given by $B_1(t)$ and $B_2(t)$, respectively, at time zero (see appendix).

DISCUSSION OF RESULTS

The model is applied to study the short-term creep behavior of Nicalon-SiC composites which have the following properties: E_f=180GPa, E_m=380GPa, ν_f=0.2, ν_m=0.18 and Poisson's ratio for fiber creep ν_{fc}=0.4. The fiber volume fraction f=0.4, fiber radius R=7μm. According to Evans (1994), the matrix of unidirectional Nicalon-SiC composites starts to undergo periodic cracking at about 122MPa. At about 250MPa, matrix cracking saturates at 9.5 cracks per mm. Over the matrix cracking stress range, the crack density varies fairly linearly with the applied stress. Previous studies (e.g., Budiansky et al., 1986) have shown that, in general, the matrix cracking stress depends on the composite residual misfit strains and the interface conditions. Although this necessitates selecting consistent values for residual misfit, friction coefficient and interface debonding energy, values for parameters are not available. El-Azab (1994) used the following parameters, which are adopted here: Coulomb friction coefficient μ=0.1, interface debonding energy $\Im_d$= 0.05 $\Im_m$ where $\Im_m$=50J/m^2, and misfit values in the

range (ε_{th} = -500 to -700 $\mu\varepsilon$), which corresponds to a difference in thermal expansion coefficient of 10^{-6} K^{-1} and a temperature changes in the range 500-700 °C.

Figure 3 shows the short-term creep behavior of Nicalon-SiC composites as a function of temperature and stress, in the absence of matrix cracks (Eq. (26)). The load 140MPa is above the matrix cracking stress. It is included here to show the trends in composite creep at such high loads if matrix cracking is not allowed. It will be shown later that the presence of matrix cracks causes much higher creep strains even under lower loads. Figure 3 shows that the creep strain is a monotonically increasing function of time. This, however, is not always the case at lower stress. In fact, the composite creep strain may be a decreasing or increasing function of time depending on the relative effects of the applied load versus the misfit effects. At low applied stress and high misfit values, the overall strain of composite with an intact matrix can be a decreasing function of time. The ultimate creep strain of composites in the absence of matrix cracks is determined by the fiber viscoelastic behavior. If the stresses in the fiber can be completely relaxed due to creep, then the ultimate creep strain of the composite is bounded by the matrix strain corresponding to the applied load. Figure 4 shows the creep behavior of the composite loaded at 130MPa with matrix cracking (Eq. (25)). In this case, fibers carry the applied load at the matrix crack surface and interface debonding takes place. Fibers creep is faster over the debonded length, which leads to further relaxation of the matrix clamping over the debonded zone and, in turn, accelerates the overall creep of the composite. As the misfit is severely relaxed, debond cracks propagate faster, which leads to a tertiary creep mode for the composite. This mode is characterized by unstable interface debonding. As the debond length ℓ approaches the mean guage length L, the composite creep rate is found to be faster than the bare fiber creep rate (subject to $\sigma_f = \sigma_a / f$) because matrix clamping around fiber is not completely relaxed.

The trends in composite creep as the debond length ℓ approaches the guage length L depends on the relative speeds of relaxation of the interface pressure (which leads to loss of interface contact) and debonding propagation speed. If debonding propagates faster, which is expected to happen at higher applied stresses, the debond length ℓ approaches L prior to complete relaxation of the interface pressure. Under such circumstances, the creep strain of the composite can reach values which are higher than those of the bare fiber. This can be attributed to the fact that fibers are subject to radial and azimuthal compression which assists axial deformation. On the other hand, if relaxation of the interface compression is faster than debonding propagation, which is expected to take place at lower applied stress, loss of contact can take place before ℓ approaches L. Prior to loss of contact, the composite creep strain is contributed partly by the accelerated fiber creep below the debond front and partly by the composite creep above the debond front which is limited by matrix clamping. Figure 5 illustrates these effects. The corresponding debonding behavior is shown in Figure 6. The effect of temperature on creep of the composite is shown in Figure 7. In general, it is observed that the lower the temperature the longer it takes to severely propagate debonding, and in turn the tertiary creep stage is delayed.

In Figure 8, the effect of the residual misfit on composite creep is shown, where the onset of unstable interface debonding is delayed at higher misfit strains. Adjusting the value misfit strain, which is usually difficult to control, represents a trade-off in optimizing ceramic composites. The optimum values of misfit for maximum matrix cracking stress are given by Budiansky et al. (1986). At high-temperatures, however, it is usually desired that the composite has as much misfit as possible to sustain loads for longer periods, which seems to be detrimental to other composite properties. In some applications, such as fusion, heterogeneous materials such as Nicalon-SiC composites will be subject to differential time-dependent dimensional changes between fibers and matrix, as well as differences in creep rates between fibers and matrix. This would require special optimization techniques to control the overall behavior of the composite.

Following the tertiary creep regime observed here, which is attributed to unstable interface debonding, the composite is expected to follow the bare fiber creep response since the end of this stage means complete loss of contact between fibers and matrix. Therefore, a stable creep regime is expected to start following this regime, during which the actual composite failure will be completely determined by the fiber failure. It is to be mentioned here that the tertiary creep in metals leads to rupture.

Eq. (25) shows that the creep of composites with matrix cracks can be represented in the form

$$\bar{\varepsilon}_c(t) = \sigma_a J_1(L(\sigma_a), \ell(t, \sigma_a), t) + \varepsilon_{th} J_2(L(\sigma_a), \ell(t, \sigma_a), t) - \varepsilon_o \quad (29)$$

where J_1 and J_2 depend on temperature as well. Generally, J_1 and J_2 are non-linear functions of the applied stress since the guage length L and the debond length ℓ depend non-linearly on the applied stress. It must be noted that these two function depend the creep temperature as well. Prior to matrix cracking loads, Eq. (26) implies that the creep strain of the composites depend linearly on the applied stress and the misfit strain. These observations should be considered in characterizing creep of such ceramic composites.

CONCLUSIONS

A micro mechanical model is developed to study the effects of fiber creep on the interface debonding and frictional slip in ceramic matrix composites. The model is applied to study the short-term overall creep behavior of unidirectional fiber composites at high temperatures which are loaded beyond the matrix cracking stress. It is found that the overall response is characterized by a secondary creep regime followed by a tertiary creep regime during which the interface debonding and slip dominates the creep behavior of the composite. This tertiary regime is characterized by loss of contact between the fiber and matrix due to relaxation of the interface pressure and severe debonding of the interface, which represents instability (softening) mechanisms associated with the tertiary creep regime.

ACKNOWLEDGMENT

This material is based upon work supported by the U. S. Department of Energy under award number DE-FG03-91ER45115.

REFERENCES

Aveston, J., Cooper, G. A. and Kelly, A., 1971, " Single and Multiple Fracture," *Proceedings, The Properties of Fiber Composites*, National Physical Laboratory, Guildford, IPC Science and Technology Press Ltd., pp . 15-26.

Aveston, J. and Kelly, A., 1973, " Theory of Multiple Fracture of Fibrous Composites," *Journal of Materials Science*, Vol. 8, pp. 352-362.

Budiansky, Bernard, Hutchinson, John W. and Evans, A. G., 1986, " Matrix Fracture in Fiber-Reinforced Ceramics," *Journal of the Mechanics and Physics of Solids*, Vol. 34 No. 2, pp. 167-189.

Carter Jr., C. H. and Davis, R. F., 1984, " Kinetics and Mechanisms of High-Temperature Creep in Silicon Carbide: II Chemically Vapor Deposited," *Journal of the American Ceramic Society*, Vol. 67 No. 11, pp. 732-740.

DiCarlo, J. A. and Morscher, G. N., 1991, " Creep and Stress Relaxation Modeling of Polycrystalline Ceramic Fibers," *ASME*, AD 22, AMD 122, pp. 15-22.

DiCarlo, J. A., 1994, " Creep Limitations of Current Polycrystalline Ceramic Fibers," *Composites Science and Technology*, Vol. 51, pp. 213-222.

El-Azab, Anter A., 1994, " Time-Dependent High-Temperature Fracture of Ceramic Matrix Composites," Ph.D. Dissertation, University of California, Los Angeles.

El-Azab, A. and Ghoniem, N. M., 1995, " Investigation of Incubation Time for Sub-Critical Crack Propagation in SiC-SiC Composites," *Journal of Nuclear Materials*, In press.

Evans, A. G. , 1994, " Micromechanics of Ceramic & Composite Strength," *1994 Institute for Mechanics and Materials Summer School-The Mechanics-Materials Linkage*, University of California, San Diego.

Gao, Yu-Chen, Mai, Yiu-Wing and Cottrell, Brian, 1988, " Fracture of Fiber-Reinforced Materials," *Journal of Applied Mathematics and Physics (ZAMP)*, Vol. 39, pp. 550-572.

Gulden, T. D. and Driscoll, C. F., 1971, " Creep of Chemically Vapor Deposited Beta-SiC With an Analysis of Creep in Bending," *Gulf General Atomic Report*, GA-1036, February 16.

Henager, C. H. and Jones, R. H., 1993, "High-Temperature Plasticity Effects in Bridged Cracks and Subcritical Crack Growth in Ceramic Composites," *Materials Science and Engineering A*, Vol. 166, pp. 211-220.

Hutchinson, John W. and Jensen, Henrik M., 1990, " Models of Fiber Debonding and Pullout in Brittle Composites With Friction," *Mechanics of Materials*, Vol. 9, pp. 139-163.

Hutchinson, John W., 1994, " Micromechanics of Ceramic Matrix Composites," *1994 Institute for Mechanics and Materials Summer School-The Mechanics-Materials Linkage*, University of California, San Diego.

Kelly, A., 1976, " Composites With Brittle Matrices," *Frontiers in Materials Science*, L. E. Mura and C. Stein, ed., Marcel Dekker, New York, pp. 335-364.

Kim, Jang-Kyo, Baillie, C. and Mai, Yiu-Wing, 1991, " Interfacial Debonding and Fiber Pull-out Stresses. Part I: Critical Comparison of Existing Theories and Experiments," *Journal of Materials Science*, 27, pp. 3143-3154.

Marshall, D. B., Cox, B. N. and Evans, A. G., 1985, " The Mechanics of Matrix Cracking in Brittle-Matrix Fiber Composites," *Acta Metallurgica*, Vol. 33 No. 11, pp. 2013-2021.

Najmabadi, F., Conn, R. W. and the ARIES Team, 1995, " The ARIES II and ARIES IV Second Stability Tokamak Reactor Study: Final Report," UCLA-PPG 1461, University of California, Los Angeles.

Pipkin, A. C., 1986, " Lecture Notes on Viscoelasticity Theory," *Springer-Verlag*.

Schapery, R. A., 1962, " Approximate Methods of Transform Inversion for Viscoelastic Stress Analysis," *Proceedings of the Fourth U.S. National Congress of Applied Mechanics*, ASME Publications, pp. 1075-1085.

Sigl, L. S. and Evans, A. G., 1989, " Effects of Residual Stresses and Frictional Sliding on Cracking and Pull-out in Brittle Matrix Composites," *Mechanics of Materials*, Vol. 8, pp. 1-12.

Zhou, Li-Min, Kim, Jang-Kyo and Mai, Yiu-Wing, 1991, " Interfacial Debonding and Fiber Pull-out Stresses. Part II: A New Model Based on Fracture Mechanics Approach," *Journal of Materials Science*, 27, pp. 3155-3166.

APPENDIX

This appendix includes the constants and functions which are used throughout the text.

c_o and c_1 first appeared in Eq. (12):

$$c_o = -\frac{c_3}{c_4},$$

$$c_1 = \frac{c_2 - E_f f v_m}{c_4}.$$

c_2, c_3 and c_4 first appeared in Eq. (15):

$$c_2 = E_m (1 - f) v_f,$$

$$c_3 = E_m (1 - f) E_f,$$

$$c_4 = E_m (1 - f)(1 - v_f) + E_f [1 + v_m + f(1 - v_m)].$$

$A_1(t)$, $A_2(t)$, $B_1(t)$ and $B_2(t)$ first appeared in Eq. (19):

$$A_1(t) = E_f\left[a_1(t) - \nu_m a_2(t)\right] / \Delta,$$
$$A_2(t) = E_f\left[-b_1(t) + \nu_m b_2(t)\right] / \Delta,$$
$$B_1(t) = E_f E_m(1-f)\left[a_1(t) - a_2(t)\right] / \Delta,$$
$$B_2(t) = E_f E_m(1-f)\left[b_2(t) - b_1(t)\right] / \Delta,$$
$$\Delta = a_1(t)b_2(t) - a_2(t)b_1(t),$$
$$a_1(t) = c_4 + c_3(1-\nu_{fc})J(t),$$
$$a_2(t) = -2[c_2 + E_f f\nu_m] - 2c_3\nu_{fc}J(t),$$
$$b_1(t) = -c_1c_4 - c_3\nu_{fc}J(t),$$
$$b_2(t) = fE_f + (1-f)E_m - c_3J(t).$$

$S_o(t)$, $S_1(t)$, $S_2(t)$, $P_1(t)$, $P_2(t)$, $R_o(t)$, $R_1(t)$, $R_2(t)$, $Q_1(t)$ and $Q_2(t)$ first appeared in Eq. (25) and used in Eq. (26):

$$S_o(t) = \frac{1}{fE_f} - \frac{\alpha_2(t)}{\alpha(t)fE_f} + \frac{J(t)}{f},$$
$$S_1(t) = \frac{\alpha_2(t)}{fE_f}\left(\frac{1}{\alpha(t)} - 2\nu_f\right),$$
$$S_2(t) = \frac{\alpha_2(t)}{f}\left(\frac{1}{\alpha(t)} - 2\nu_{fc}\right),$$
$$R_o(t) = -\frac{\alpha_1(t)}{\alpha(t)E_f},$$
$$R_1(t) = \frac{\alpha_1(t)}{E_f}\left(\frac{1}{\alpha(t)} - 2\nu_f\right),$$
$$R_2(t) = \alpha_1(t)\left(\frac{1}{\alpha(t)} - 2\nu_{fc}\right),$$
$$P_1(t) = \left[A_1(t) - 2\nu_f A_2(t)\right] / E_f,$$
$$P_2(t) = \left[A_1(t) - 2\nu_{fc}A_2(t)\right],$$
$$Q_1(t) = \left[B_1(t) - 2\nu_f B_2(t)\right] / E_f,$$
$$Q_2(t) = \left[B_1(t) - 2\nu_{fc}B_2(t)\right].$$

FIGURES

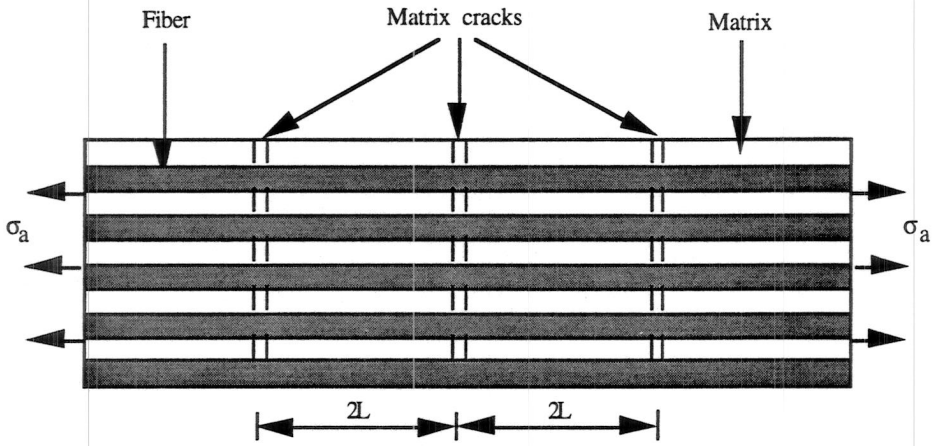

FIGURE 1: SCHEMATIC SHOWING PERIODIC MATRIX CRACKS IN UNIDIRECTIONAL COMPOSITES.

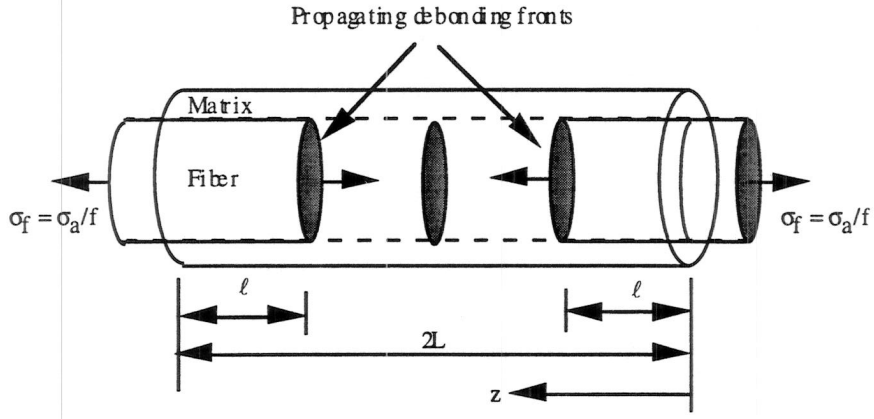

FIGURE 2: CYLINDRICAL CELL MODEL.

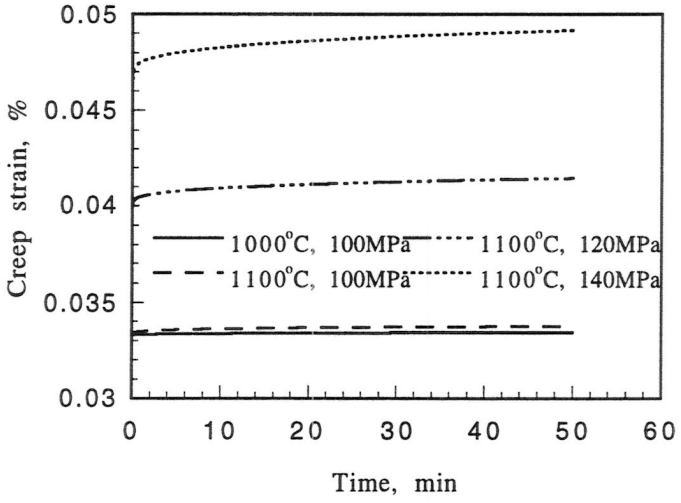

FIGURE 3: CREEP OF NICALON-SiC COMPOSITES WITH NO MATRIX CRACKS.

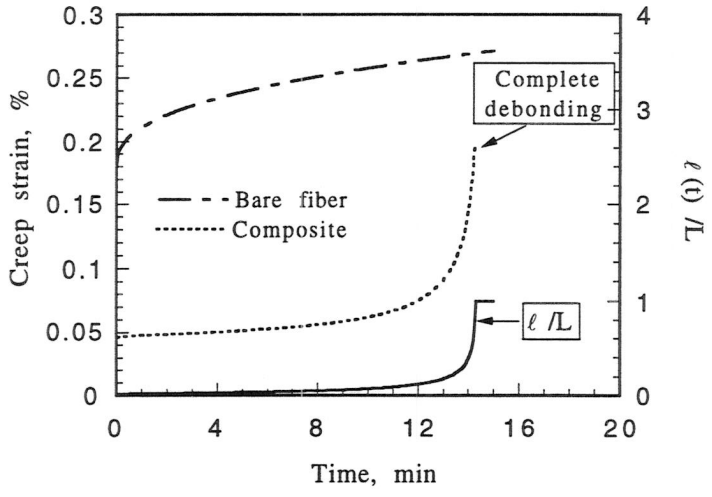

FIGURE 4: CREEP OF FIBER AND CRACKED COMPOSITE AT 1100 °C AND 130MPa . THE INSTANTANEOUS DEBOND LENGTH IS ALSO SHOWN.

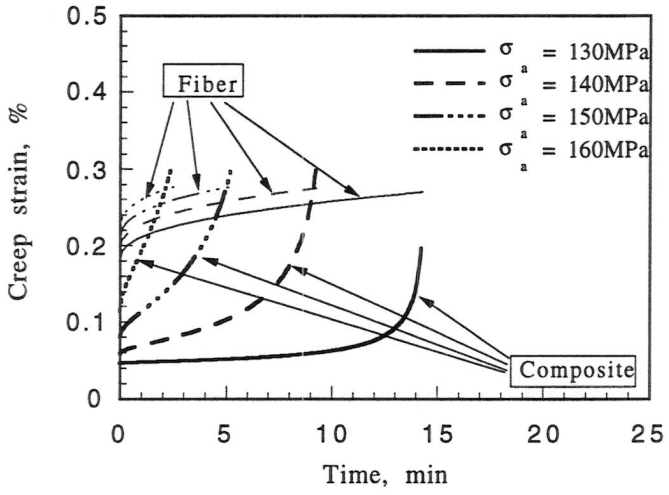

FIGURE 5: COMPOSITE AND FIBER CREEP STRAIN AS FUNCTION OF TIME AND APPLIED STRESS AT 1100 °C. (MATRIX IS CRACKED).

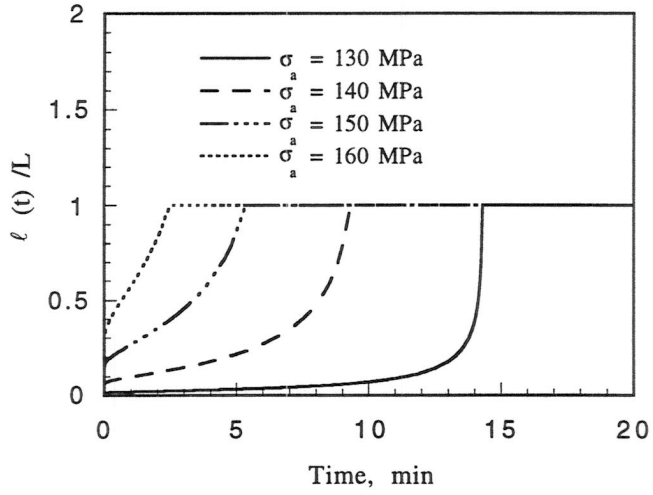

FIGURE 6: EFFECT OF APPLIED STRESS ON THE DEBONDING PROPAGATION IN NICALON-SiC COMPOSITES AT 1100°C.

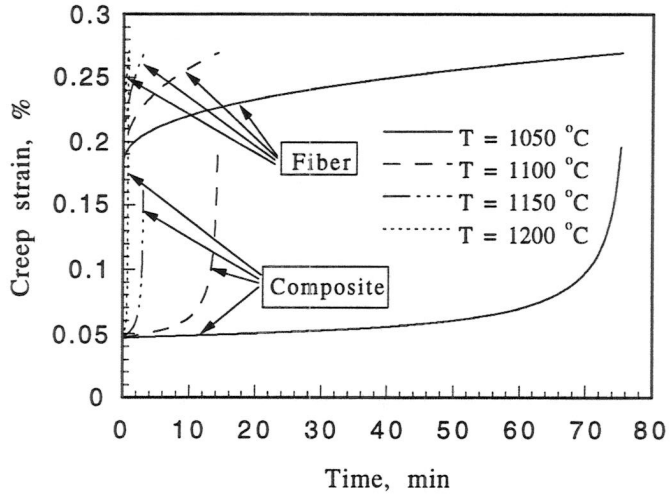

FIGURE 7: EFFECT OF TEMPERATURE ON COMPOSITE CREEP AT 130MPa.

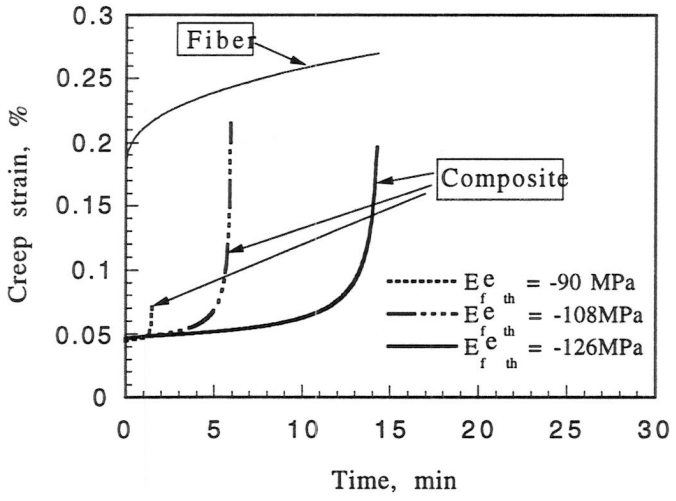

FIGURE 8: EFFECT OF MISFIT STRAIN ON CREEP OF NICALON-SiC COMPOSITES AT 1100°C AND 130MPa.